Research Paper

Influence of Beam Height-Column Width Ratio on Seismic Behavior of RC Moment Resisting Frames

Ali Khalili[1] and Fariborz Nateghi-Alahi[2*]

1. Ph.D. Student, International Institute of Earthquake Engineering and Seismology (IIEES), Tehran, Iran
2. Professor, Structural Engineering Research Center, International Institute of Earthquake Engineering and Seismology (IIEES), Tehran, Iran,
*Corresponding Author; email: nateghi@iiees.ac.ir

Received: 03/09/2023
Revised: 23/12/2023
Accepted: 14/01/2024

ABSTRACT

Most reputable international design codes have included provisions for achieving ductile behavior and avoiding brittle and hazardous behavior in reinforced concrete frames. These provisions aim to achieve the concept of weak beam-strong column, where plastic hinges during earthquake occur first in the beams. Analysis of frequent and repetitive failures in strong earthquakes in recent decades of reinforced concrete structures shows that the strong beam-weak column failure mode typically leads to severe damage in these structures. The frequent occurrence of this failure mode can be attributed to two main factors. Firstly, stiffer beams are often used against more flexible columns due to the absence of seismic provisions that limit the relation between beam height and column width results in column severe damage on column and finally collapse of them. Secondly, the effect of the cast-in-situ slab in increasing the negative flexural strength of the beam is often underestimated or ignored, leading to the flexural strength of the columns being less than that of the beams. To assess the impact of the ratio of beam height to column width on the seismic performance of MRFs, a series of computational models were created and analyzed in a parametric study. Prior to that, the FEA performance was validated by comparing its results with experimental data. The findings emphasize the urgent need for a new seismic provision that limits the beam height to column width ratio to a maximum of 1.25

Keywords:
Ratio of beam height to column width; RC MRFs; Finite element analysis; Effective slab width

1. Introduction

One of the most common structural systems used in multi-story buildings is reinforced concrete (RC) moment-resisting frames (MRFs) with various types of ductility. It is reported that the "weak column-strong beam" failure mode in strong earthquakes in recent decades has been one of the most frequent types of failures in RC MRFs (Arslan & Korkmaz, 2007; Dogan, 2013; Zhao et al., 2009; Rossetto et al., 2011; Rossetto & Peiris, 2009; Yan et al., 2010).

The occurrence of this failure results in the formation of plastic hinges on columns, which may finally cause the collapse of the structure. Also, it may make them unrepairable or cause significant difficulties in utilization. This failure mode is named column-driven mechanism, which is unfavourable based on capacity design philosophy (Paulay & Park, 1975). In this way to avoid Collapse due to the column-driven mechanism, the summation of the flexural strength of columns shall be greater than beams the junction with which is named as "strong column-weak beam"

(SCWB) design method (Masoudi & Khajevand, 2020).

Some of the reasons that cause the mentioned type of failure in RC MRFS are discussed in the literature. Arslan and Korkmaz (2007) stated that defining deeper beams and flexible columns in the design and construction of RC MRFs in Turkey due to defining long spans causes the beams to remain elastic while the columns experience failure due to the compression crushing or shear failure during seismic lateral loading (Arslan & Korkmaz, 2007). Based on the main observations reported by Dogan, the major reasons for Columns' damage were due to inadequate cross-sectional dimensions of them, using rectangular section columns, and excessive beam strength due to the height of the cross-section (Dogan, 2013). It could be concluded that the geometrical dimension of beams and columns may affect the failure mode of "Strong beam-Weak column".

In the recent earthquake that happened in 2023 in Kahramanmarash, Turkey, many buildings partially or completely collapsed due to strong beam-weak column deficiencies. Using thin and narrow columns in the construction of RC MRFs caused them to fail, ultimately leading to the collapse of whole structures, as shown in Figure (1). In 2017, the Sarpol-e Zahab region in Kermanshah province, Iran was struck by a significant earthquake. Based on reported observations, one of the most common modes of failure was identified as the "strong beam-weak column" failure mode. This type of destruction is demonstrated in Figures (2) and (3).

The structures which experienced partial or overall collapse due to "strong beam-weak column" failure mode, in the Sarpol-e-Zahab earthquake, were particularly designed based on the ninth section of the 2013 edition of Iran's national building regulations (INBR) or older revisions (Iranian National Building Codes, 2013).

Three categories have been considered by (Iranian National Building Codes, 2013) for the seismic design of RC MRFs ordinary, intermediate, and special ductility. Unfortunately, in practice, most designers carried out the design of these building frames with intermediate ductility due to the complexity of special ductility provisions

Figure 1. Collapse of a residential building due to column failure (Sezen et al., 2023).

Figure 2. Spalling of column concrete and undamaged beams (Vetr et al., 2018).

Figure 3. Lateral sway mechanism caused by formation of hinges on columns (Vetr et al., 2018).

(Vetr et al., 2018). Additionally, (Iranian National Building Codes, 2013) does not consider any requirement to satisfy the "SCWB" design method in reinforced concrete frames with ordinary and intermediate ductilities.

Therefore, to achieve a reduction in the "lateral relative displacement of floors" below the maximum values stipulated by seismic loading regulations, designers often increase the cross-sectional height of the beams. Also, designers may opt to incorporate long spans with rectangular section columns for architectural reasons, resulting in an increased cross-sectional height of the beams. While this design approach can improve the stiffness and flexural capacity of the beams, it may also lead to damage accumulation at the column ends during seismic events such as Sarpol-e Zahab.

It should be noted that current seismic design regulations for reinforced concrete structures, such as the 9th section of INBR, ACI-318 (2019), and EuroCode 8 (2004), do not include provision for the "beam height to column width" ratio in frame design.

On the other hand, many experimental and numerical studies have examined the effect of various parameters on the accomplishment of the strong column-weak beam design methodology, and have concluded that the ratio of the summation of column flexural strength to beam flexural strength at a joint, as proposed by codes such as ACI-318 (2019) and EuroCode 8 (2004), is not adequate (Dooley & Bracci, 2001; Kuntz & Browning, 2003; Medina & Krawinkler, 2005; Ibarra & Krawinkler, 2005; Haselton et al., 2001). It could be argued that considering the summation of flexural strength of columns of a junction greater than beams of such connection is not the proper solution to gain SCWB design methodology in practice. It seems there is a need to determine minimum criteria to eliminate the geometrical dimensions of the beam and column to prevent column hinge formation during lateral seismic loadings.

One of the other reasons why RC MRFs tend to exhibit column-driven failure mechanisms during strong earthquakes worldwide is the disregard or undervaluation of slab contribution by building codes.

In the case where beams are cast monolithically with slabs, the slab reinforcements act as additional flexural reinforcement for the beam, which is known as the slab contribution, when the beam is bent and the slab is under tension (Pantazopoulou et al., 1988). This may cause the beam strength to exceed that of the column, thus affecting the seismic performance of the RC MRF and hindering the accomplishment of the "SCWB" design methodology (Paulay & Park, 1975; Masoudi & Khajevand, 2020; Pantazopoulou et al., 1988; Kabeyasawa & Kabeyasawa, 2018; Pantazopoulou, 1991). To accurately determine the contribution of the slab, an appropriate effective slab width must be defined.

It is indicated that the values of effective slab width prescribed by seismic design codes, such as ACI 318 (2019) and EuroCode 8 (2004), are not sufficient for achieving "SCWB" design methodology among several recent studies (Paulay & Park, 1975; Pantazopoulou et al., 1988; Kabeyasawa & Kabeyasawa, 2018; Pantazopoulou, 1991; Myoungsu & LaFave, 2004; Umarani & Ahmed, 2014).

Based on the above-mentioned points and the authors' best knowledge, there is a pressing need to evaluate the impact of the beam height to column width ratio and the effect of slab of RC MFRs on the attainment of the 'SCWB' design approach.

In light of this, a set of computational models was developed using finite element analysis (FEA), based on the experimental investigation conducted in Ning et al., (2014), to evaluate the influence of connection geometrical characteristics on the failure mechanism and seismic performance of spatial RC MRFs while accounting for their continuity. Once the modeling procedure for 3D RC MRFs using the FEA software ABAQUS was outlined, the accuracy of the finite element (FE) model was verified by comparing the results predicted by ABAQUS with the experimental findings from (Ning et al., 2014). The parametric study focused on longitudinal (beam and loading are in the same direction), main beam height, and width of column by preparing eighteen 3D spatial RC MFRs in ABAQUS. The 3D spatial RC MRF models were subjected to loading and analyzed

using the unidirectional nonlinear static procedure. The effective slab width obtained from the finite element analysis (FEA) was then compared to the values prescribed by ACI 318 (2019) and EuroCode 8 (2004).

2. Numerical Modeling

2.1. Experimental Background

The current paper utilizes an experimental study conducted by Ning et al. in 2014 to develop a Finite Element (FE) model in ABAQUS for the purpose of verification. The experimental investigation by (Ning et al., 2014) comprised of two 1/2-scale 3D RC MRFs, namely RC-1 and RC-2. Both specimens had two stories and two longitudinal spans, along with one span in the transverse direction. The width of both longitudinal and transversal beams is 100 mm, and the overall height of mentioned beams is 200 mm. Slab thickness equals 50 mm, and the cross-section of columns is 160×160 mm^2. The overall height of RC-2 is 3280 mm, and the height of each story equals 1440 mm.

The length of the transverse span is 1600 mm, and the length of the longitudinal spans are 2400 and 1600 mm. RC-1 lacked a slab, whereas RC-2 had a cast-in-situ slab. Figure (4) represents the geometry of RC-2 in detail. As shown in Figure (5), two actuators transferred static cyclic loads to the top of RC-2. The lateral load history was displacement control with three equal amplitude cycles. The amplitude of cycles increased sequentially during loading.

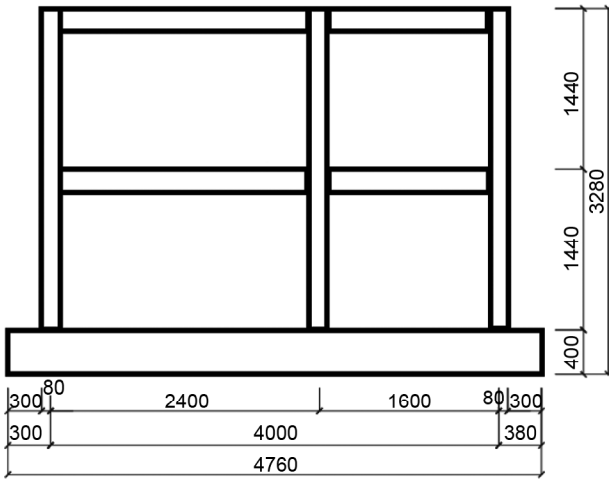

Figure 4. Elevation view of RC-2 (Ning et al., 2014).

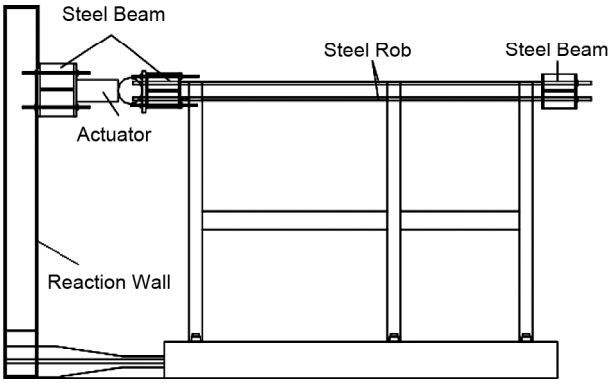

Figure 4. The setup of lateral loading (Ning et al., 2014).

2.2. Finite Element Modeling Methodology

For the simulation of RC-2 in ABAQUS, a modeling technique was employed, which utilized eight-node brick elements with reduced integration for representing the concrete, and two-node linear truss elements for representing the steel reinforcement. The brick elements were utilized to model the host region, while the embedded region represented the reinforcement, enabling perfect bonding between the steel and concrete. In order to impose boundary conditions in the FE model, the transitional degree of freedom at the end face of columns in the first story was constrained to zero, in accordance with the experimental setup. Additionally, lateral displacements in opposite directions were applied to the second story of RC-2, as per the experimental conditions. For the concrete part of the FEA model, two different mesh sizes were utilized. The slab thickness was discretized using five eight-node brick elements, each with a volume of 50 × 50 × 10 mm3, where 10 mm represented the thickness of each element. The mesh size for the remaining parts of the model was set at 50 mm. The mesh, reinforcement, and boundary conditions of the ABAQUS FEA model are illustrated in Figure (6).

2.3 Material

2.3.1. Concrete

Concrete damaged plasticity (CDP) was hired to simulate the nonlinear behavior of concrete. CDP definition in ABAQUS (2013) is based on three essential sections: plasticity parameters, uniaxial behavior of concrete in compression and tension, and damage variables.

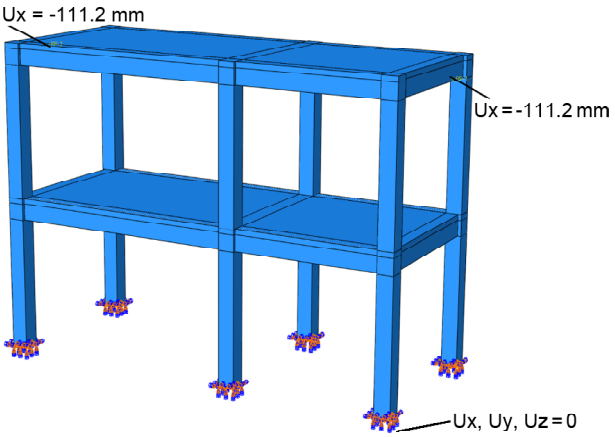

Figure 6. FE Model of RC-2, Boundary Condition.

Modeling the uniaxial behavior of concrete and assessing damage in both tension and compression is defined by a methodology developed by Alfarah et al. (2017). The authors validated the mesh-insensitivity of their proposed model. In this way, the mesh sensitivity was ignored in present study. The main aspects of the model, with some modifications, are outlined below:

The yield functions in stress space is a function of two parameters which are defined as biaxial compressive yield stress to uniaxial compressive yield stress ratio that influences the yield surface in a plane stress condition (f_{b0} / f_{c0}), and the ratio of distances between the hydrostatic axis and compression meridian and tension meridian in the deviatoric cross-section which is interpreted as K_c. The ABAQUS user's manual specifies default $f_{b0} / f_{c0} = 1.16$. Also, physically, it is highly recommended to assume $K_c = 2/3$ (ABAQUS, 2013).

The CDP model used in ABAQUS software is a modification of the Drucker-Prager strength hypothesis. It is based on the assumption of non-associated potential plastic flow. The Drucker-Prager hyperbolic function gives the flow potential

$$G = \sqrt{(\epsilon \sigma_{t0} \tan\psi)^2 + q^2} - p \tan\psi \quad (1)$$

In Equation (1) σ_{t0} is the uniaxial tensile stress at failure, ϵ is eccentricity. It can be calculated as a ratio of tensile strength to compressive strength. It is recommended to assume $\epsilon = 0.1$ (ABAQUS, 2013). Physically, dilation angle ψ is interpreted as a concrete internal friction angle (Alfarah et al., 2017; Khalili et al., 2015; Kheyroddin et al., 2020). Dilation angle for concrete ranges from 15 to 56 based on the literature (Lubliner et al., 1989; Behnam, 2018; Lee & Fenves, 1998). The Poisson's ratio was set as 0.2. Also, viscoplastic regularization was considered 0.0001 s to avoid convergence difficulties due to the softening behavior of concrete.

In FE model, the dilation angle was found to have two different values because the elements in the first story experienced higher stress levels compared to the second story. A sensitivity analysis was conducted to determine the best values that would fit the experimental results more accurately. Based on the sensitivity analysis, the dilation angles for the first and second stories were chosen to be 45 and 40, respectively.

The stress-strain model for multi-axial condition, in the CDP model, is based on a basic model that uses scalar damage, and effective stress to create coupling between damage and plasticity is given by Equation (2):

$$\sigma = (1-d) D_0^{el} : (\varepsilon - \varepsilon^{pl}) \quad (2)$$

where σ denotes the true stress, D_0^{el} is the initial (undamaged) elastic stiffness, ε and ε^{pl} are the total and plastic strain, respectively. Effective stress is defined as $\bar{\sigma} = D_0^{el} : (\varepsilon - \varepsilon^{pl})$. Parameter d is a damage variable ranging from 0 (no damage) to 1 (maximum damage) (destruction). Based on Figure (7), the stress-strain relations for damaged concrete under uniaxial compression and tension loading are defined as below:

$$\sigma_c = (1-d_c) E_0 (\varepsilon_c - \varepsilon_c^{pl}) \quad (3)$$

$$\sigma_t = (1-d_t) E_0 (\varepsilon_c - \varepsilon_t^{pl}) \quad (4)$$

ε_c^{pl} and ε_t^{pl} are hardening variables for compression and tension, respectively. Tensile and compression Damage variables (d_c and d_t) in this study are obtained from the approach presented and implemented by Alfarah et al. (2017).

The definition of uniaxial behavior and evaluation of damages in both tension and compression of concrete is defined based on a methodology implemented by Alfarah et al. (2017). Figure (7a) represents the Stress-strain curve of concrete in the compressive part, follows a linear function until $0.4 f_{cm}$. After this point, a nonlinear and increasing part of the curve begins

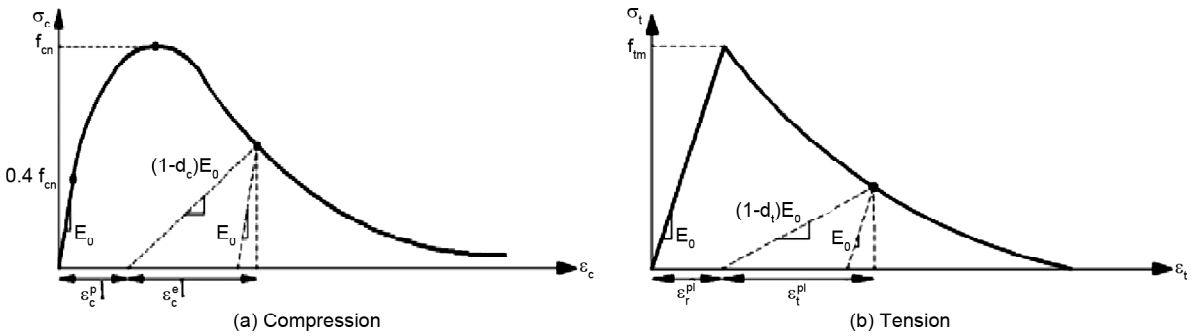

Figure 7. The proposed stress-strain relationship of concrete under uniaxial compression and tensile.

Table 1. Steel bar's mechanical details.

The Steel Part of the Cage	Modulus of Elasticity (MPa)	Diameter (mm)	Yield Strength (MPa)	Tensile Strength (MPa)
Column Longitudinal Bars	156000	10	384	508
Beam Longitudinal Bars	168000	8	304	423
Slab Bars	151000	6	294	401
Stirrups	151000	6	294	401

and continues until f_{cm} (compressive Stress strength), that its corresponded strain is ε_{cm}.

As shown in Figure (7b), the stress-strain curve of concrete in tensile portion follows a linear function to get to f_{tm} (tensile stress strength). Corresponding strain to tensile strength is ε_{tm}. Equation (5) represents the relation between f_{tm} and f_c':

$$f_{tm} = 0.316 f_c'^{2/3} \quad (5)$$

After this point, cracks appear in the concrete, and the curve softens, causing localized strains and increased crack width (ABAQUS, 2013).

Compression damage values are calculated in the crushing strain range, which starts at the $0.4 f_{cm}/E_0$ value at the end of the linear segment. Tensile damage values are calculated for the softening part and are assumed to originate from strain, which corresponds to tensile strength (f_{tm}).

2.3.2. Steel

A trilinear elastic-plastic behavior was used for steel reinforcement. The module of elasticity (E_s), and Poisson's ratio (υ) are elastic parameters of steel. υ is considered equal to 0.3 and E_s was defined based on data was provided in (Ning et al., 2014). Table (1) summarizes the primary mechanical properties of the steel bars employed in the construction of RC-2.

3. Verification of FE Model

3.1. Load-Displacement Curve

Figure (8) presents a comparison between the load-displacement response obtained from the experimental test and the prediction of the FE model. The predicted response from the FEA is fitted to the experimental results. Table (2) provides a comparison between the average peak lateral load and displacement of RC-2 obtained from the test and FE model. The good predictive implementation of the FE model is reflected in the robust correlation between numerical and experimental results. Even though a thorough cyclic analysis was conducted in ABAQUS, the hysteresis loops did not exhibit a pinching phenomenon

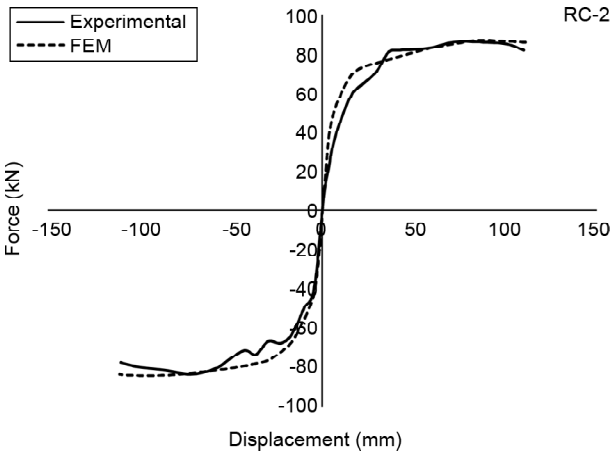

Figure 8. comparison of FEA and Experimental load-displacement response.

Table 2. Comparison test and FEA results.

Model	Peak Load Average (kN)	Peak Displacement Average (mm)
Experimental	84.25	80
FEA	85.46	86.11
Error%	1.46	7.64

akin to the test. This could be due to the definition of the ideal adhesion between concrete and reinforcements, as well as the intricacy of the constitutive modeling of concrete. As a result, this paper only presents and discusses the findings of the analysis conducted under monotonic loading conditions.

3.2. Failure Mode and Reinforcement Yielding

Simulation results indicated that, although hinges formed in beams in the early loading stage, finally RC-2 experienced strong beam-weak column failure mode due to hinge formation on the columns, as shown in Figure (9). Based on numerical observations, the middle column's panel zone of the first story experienced severe damage similar to experimental ones. Experimental results reported that transverse beam longitudinal reinforcement yielded at story drift of 3%. On the other hand, based on the prediction of the FE model, when the slab was in tension, the transverse beam's top and bottom longitudinal reinforcements (located on the inner side of the beam) yielded at story drift of 2.4% and 3.6%, respectively. Therefore, it can be inferred that there is a reasonable agreement between the values obtained from the FEA and the test.

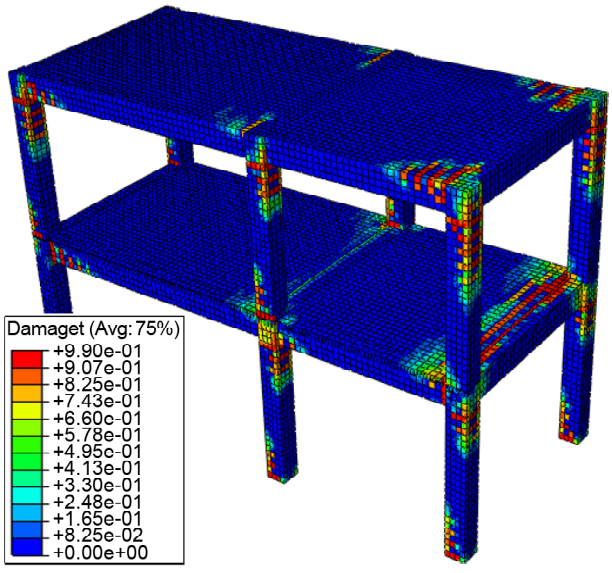

Figure 9. Hinge formation of FEA model.

3.3. Flexural Moment at Feet of Columns

Ning et al. (2014) reported the flexural moment values of the corner and middle columns at the feet based on experimental measurements of the columns' longitudinal strain at a drift of 2%. Table (3) compares these values with the corresponding FEA results. The mean absolute error is 3.47%, that indicates a strong correlation between the FEA and experimental values.

The numerical model exhibited good performance to anticipate the nonlinear behavior of RC MRF, and a close correlation was seen between numerical and test results.

4. Parametric Study

This study aims to evaluate the effect of the ratio of beam height to column width on the seismic behavior of RC MRFs while considering their continuity and the presence of slabs. Additionally, this study examines the impact of these parameters, as well as the geometric characteristics such as longitudinal beam height and length dimensions, on the effective slab width of RC MRFs, when slab is in tension. To create the FE models with different span lengths, the position of the middle frame in RC-2 was modified. By doing so, the length of longitudinal beams was set to 0.8, 1.2, 2, 2.8 and 3.2 m. The beam height of these models varied between 160 mm and 280 mm. In total, eighteen RC MRFs were modeled and analyzed. The geometric characteristics of this group are

Table 3. Flexural moment comparison between test and FEA results.

Model	Corner Column (Long Span) (kN.m)	Middle Column (kN.m)	Corner Column (Short Span) (kN.m)
Experimental	8.74	13.34	9.47
FEA	9.1	13.59	9.05
Absolute Error (%)	4.11	1.87	4.43

Table 4. Detail of FE models.

Model Name	h_{lb} (mm)	C (mm)	h_{tb} (mm)	l_{tb} (mm)	h_s (mm)	$l_{lb}(mm)$	h_{lb}/C	α_f	l_{lb}/l_{tb}	l_{lb}/h_{lb}
MFRC1-1 - MFRC1-18	160	160	200	1600	50	800	1	4.09	0.5	5
						1200			0.75	7.5
						2000			1.25	12.5
						2800			1.75	17.5
						3200			2	20
	200					800	1.25	8	0.5	4
						1200			0.75	6
						2000			1.25	10
						2800			1.75	14
						3200			2	16
	240					1200	1.5	13.82	0.75	5
						2000			1.25	8.33
						2800			1.75	11.66
						3200			2	13.33
	280					1200	1.75	21.95	0.75	4.28
						2000			1.25	7.14
						2800			1.75	10
						3200			2	11.42

h_{lb}= Longitudinal Beam Hight (mm), h_{tb}= Transverse Beam Hight (mm), l_{tb}= Transverse Beam Length (mm), l_{lb}=Longitudinal Beam Length (mm), C= Column Width, $\alpha_f \geq 0.8$ (ACI 319-19, 8.3.1.2.1)

detailed in Table (4). The variation range of geometrical characteristics is by code provisions about the aspect ratio of two-way slab, longitudinal beam length to beam depth, and beam-to-slab flexural stiffness ratio, α.It is noticeable that other design considerations related to the percentages of longitudinal and transversal reinforcements of beam, column and slab were checked by code provisions of ACI 318 (2019). The transverse beam length and height, column width, longitudinal and transverse reinforcement ratio in beams and columns, slab thickness, and longitudinal and transverse beam web width were constant. Material properties were the same as the verified model. The results obtained from FE modeling were compared with experimental results and validated at a story drift of 4.2%. To ensure that the analyses were performed within a reasonable range of lateral displacement, a story drift of 4.2% was chosen to capture the nonlinear behavior of the RC frames.

4.1. Effect of Ratio h_{lb}/C on Connection Failure Type

The failure mode at each corner joint was found to be influenced by the ratio of h_{lb}/C, according to FEA observations. Figure (10) shows the relation between h_{lb}/C and the summation of flexural moment of columns that connect at the corner joint (ΣM_c) of FE models. The values of ΣM_c were calculated for 2% story drift. The plotted results showed that as the ratio of h_{lb}/C increased from 1 to 1.75, the mean values of ΣM_c increased by 100.04% at the story drift of 2%. It could be argued that when the aspect ratio of the joint (h_{lb}/C) increases, the developed compression strut in the joint becomes steeper, resulting in a greater vertical component (D_{cy}). As shown in Figure (11), this greater vertical component induced greater compression (C_{c2} + C_{s2}) and tensile stress (Z_2) on the column face of the joint due to their equilibrium, which ultimately leads to an enhancement of flexural demand on it.

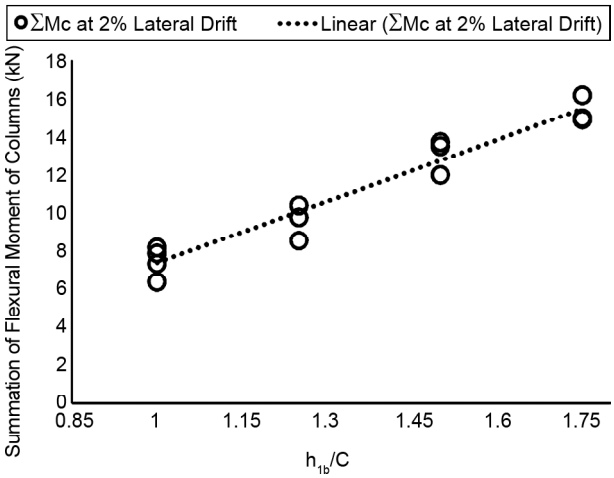

Figure 10. The trend of ΣM_c versus h_{lb}/C.

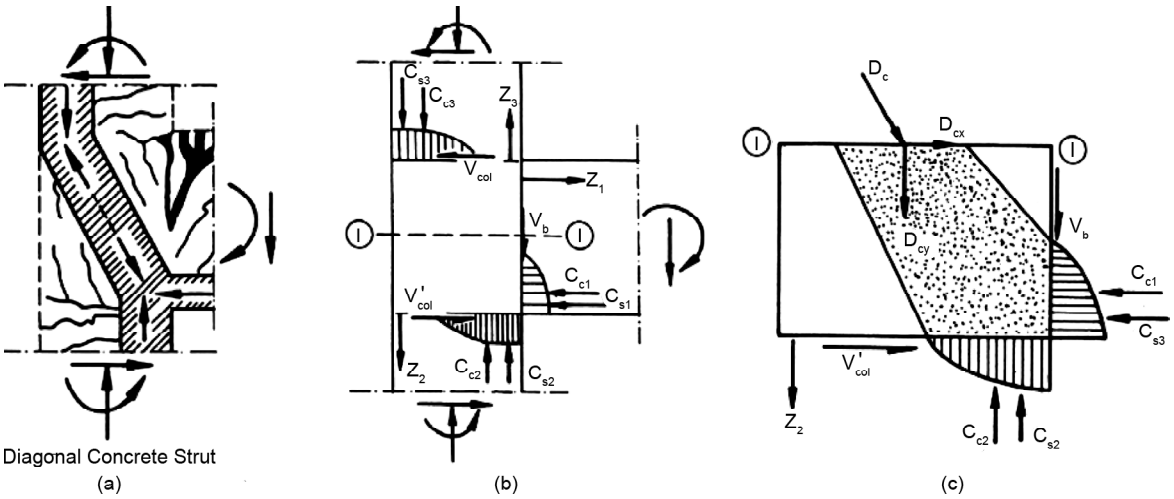

Figure 11. (a) Developed diagonal concrete strut, (b) Internal forces around an exterior beam-column joint, and (c) Forces acting in the joint core concrete through section I-I (Paulay & Park, 1975).

Table 5. Failure mode of FE models.

Model Name	h_{lb} (mm)	C (mm)	$l_{lb}(mm)$	h_{lb}/C	$\sum M_c$ (4.2%), (kN.m)	FEA Results for $\sum M_c/M_b$	Design Values of $\sum M_c/M_b$ by Considering Slab Effective Width Based on 9th INBR-2012	Failure[1]
MFRC1-1 - MFRC1-18	160	160	800	1	9.3	1.24	2.1	BT
			1200		9.31	1.24	2.15	BT
			2000		9.57	1.27	2.15	BT
			2800		8.14	1.08	2.18	BT
			3200		7.59	1.01	2.2	BT
	200		800	1.25	10.91	1	1.71	BTC
			1200		10.42	0.95	1.65	BTC
			2000		9.8	0.9	1.73	BT
			2800		10.43	0.98	1.82	BT
			3200		9.56	0.92	1.85	BT
	240		1200	1.5	13.74	0.91	1.2	BJTC
			2000		12	0.83	1.2	BJT
			2800		13.74	0.95	1.22	BTCJ
			3200		13.52	0.95	1.25	BT
	280		1200	1.75	20.23	1	1	CBJT
			2000		16.94	0.85	1	CBJT
			2800		18	0.9	1	CBJ
			3200		18.13	0.91	1	CBJ

[1] B= beam flexural failure, C = column flexural failure, J = joint shear failure, T = transverse beam failure.

Although the design values of $\Sigma M_c/M_b$ based on 2012 edition of 9th section of INBR are greater than 1.2 in the most cases of Table (5), the measured values of this ratio did not meet the "SCWB" criterion that is specified in mentioned code. On the other hand, the anticipated failure mode of the same joints by taking into account the order of occurrence is displayed in Table (5). In the case the aspect ratio of joint is greater than 1.25, when a slab existed, the flexural moment demand of columns is more that their flexural capacity, which ultimately caused plastic hinge formation on them and the failure mode of frames changed to unfavorable Strong beam-Weak column that is not suitable for implementing "SCWB" design method in practice. Thus, to prevent column hinge formation in RC MRFs, the ratio of h_{lb}/C should be limited to 1.25 within the dimensional constraints of seismic design requirements. It could be argued that, in the case of RC moment resisting

frames designed by 2012 edition of 9th section of INBR, and the ratio of beam height to column width ratio is more than 1.25, there is a possibility of experiencing unfavorable strong beam-weak column failure mode during major earthquakes. Thus, there is a need to re-evaluate such structures in order to strengthen them.

4.2. Effect of Geometric Parameters on Effective Slab Width

Figure (12) depicts the relationship between the normalized effective slab width (NESW), which is normalized to the slab thickness, and the ratio of longitudinal beam length to Transversal beam height (l_{lb} / l_{tb}). Each point belongs to a model with specific longitudinal beam height. The NESW showed a slight increase as the l_{lb} / l_{tb} ratio increased from 0.5 to 1.25. This increase is averagely 15.3% for models with different beam heights of 160 mm, 200 mm, and 240 mm. Also, results show that when the l_{lb} / l_{tb} ratio was varied in the range of 1.25 up to 2; the NESW values approximately do not vary.

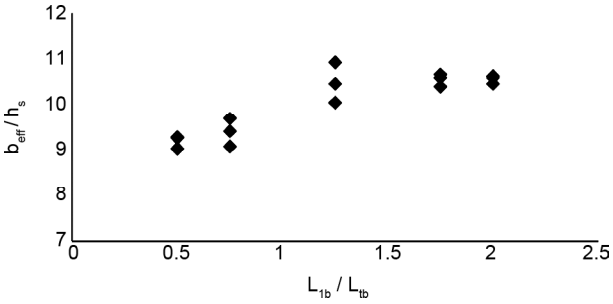

Figure 12. The trend of NESW to slab thickness versus l_{lb}/l_{tb}.

4.3. Trends of h_{lb}/C versus NESW

The results plotted in Figure (13) indicate that the beam height has a negligible effect on the value of effective slab width when the ratio of longitudinal beam height to column width (h_{lb}/C) is less than 1.5. However, for models with a ratio of h_{lb}/C equal to or greater than 1.5, the trend of NESW is different, and the mean value of NESW for models with a beam height of 280 mm is 9% to 25.3% less than other models. Furthermore, FEA shows that more shear cracks occurred in the panel zone, and transverse reinforcements of joints yielded in models with a h_{lb}/C ratio of 1.5 or greater. Figure (14) provides instances of the trend

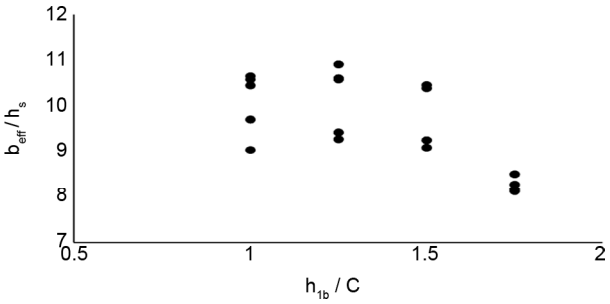

Figure 13. The trend of NESW versus h_{lb}/C.

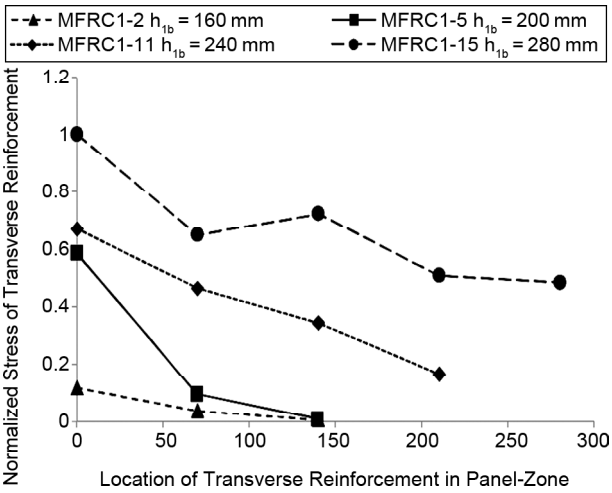

Figure 14. Effect of joint aspect ratio on stress variation across the height of joint.

of tensile stress variation of transverse reinforcements across the panel zone height in models with different beam heights. The demand for horizontal shear forces in the panel zone was calculated, considering the effective slab width. These forces had no significant variation for MFRC1-2, 7, 11, and 15, with values equal to 67.36, 65.39, 63.96 and 60.76 kN, respectively. These values are less than the shear strength of the joint based on ACI-318 provision. As illustrated in Figure (13), the transverse reinforcements belonging to the model with a beam height of 280 mm experienced more stress than other models. More tensile stress in the transverse reinforcements of the joint, while the shear forces are approximately constant, could result from losing the shear strength of the joint due to a decrease in the horizontal component of the developed compression strut. That ultimately results in less slab participation. These results suggest that for joint aspect ratios greater than 1.5, the shear strength of the joint plays a key role in decreasing slab contribution

when a slab exists. On the other hand, ACI-318 (2019) restricted the aspect ratio of the joint to 2, while this study indicated this ratio should be reduced to 1.5 in order to prevent joint shear failure.

A formula to calculate the effective slab width, Equation (6), was developed through fitting analysis. The relationship between the ratio of longitudinal beam height to column width (h_{lb}/C) and normalized effective slab width (NESW) was determined using the second-order polynomial. The coefficient of determination (R-squared value) for the equation was 0.617, indicating a strong correlation between h_{lb}/C and NESW.

$$\frac{b_{eff}}{h_s} = -6.28\left(\mathrm{h}_{lb}/\mathrm{C}\right)^2 + 14.95\left(\mathrm{h}_{lb}/\mathrm{C}\right) + 1.38 \qquad (6)$$

The current study could be considered as the first step in the research on the effect of h_{lb}/C on the failure mechanisem and shear strength of panel zone in the RC MRFs.

However, the results of this study should be considered with caution due to its numerical basis. It is suggested that future studies conduct experimental tests to verify the effect of this ratio on the collapse mechanism of RC MRFs and shear strength of panel zone. The mentioned experimental test should be conducted on a continuous RC MRF to assess the effect of slab existence.

4.4. NESW Obtained from FEA and Code Values

Figure (15) presents the normalized effective slab width (NESW) values for each FE model, along with the corresponding NESW values based on ACI code and EuroCode 8. At a story drift of 4.2%, the average NESW value obtained from FEA is 1.75 and 3.12 times greater than the average values suggested by ACI code and EuroCode 8, respectively. The results in Figure (15) suggest that the current provisions to calculate effective slab width are inadequate and may result in underestimating the actual flexural strength of beams. Regarding the failure modes obtained from numerical observation, which are presented in Table (5) and as previously discussed, this underestimation could cause a change in the failure mechanism of these RC MRFs, although they are designed based on the SCWB methodology of design.

5. Conclusions

This research paper explores the influence of geometrical parameters on the seismic performance of spatial 3D RC MRFs with slab through finite element analysis. The experimental results were compared with the measurements obtained through FEA. To investigate the effect of geometrical parameters on the effective slab width and seismic performance of models, 18 distinct finite element models were created and

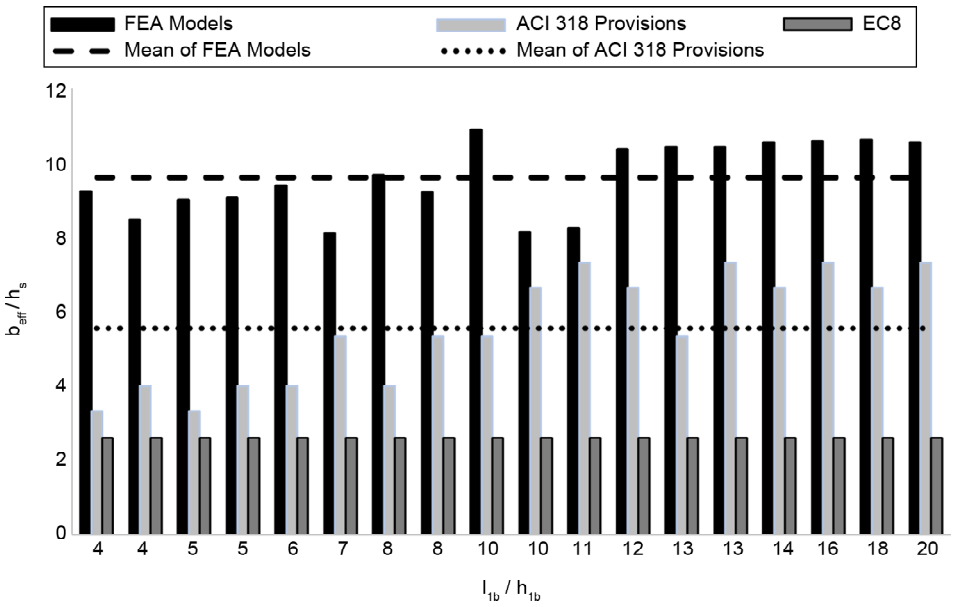

Figure 15. Comparison of NESW.

analyzed using ABAQUS. Based on the findings obtained from this numerical modeling, the following conclusion can be drawn.

- The numerical results exhibit a strong correlation with the test results.
- The findings demonstrate that the value of effective slab width is minimally impacted by the beam height when the ratio of longitudinal beam height to column width (h_{lb}/C) is less than 1.5.
- The numerical study reveals that for joint aspect ratios (h_{lb}/C) greater than 1.5, the shear strength of the joint plays a critical role in reducing slab contribution.
- This study indicates that increasing h_{lb}/C results in the enhancement of column flexural moment demand by more than 100%. This can significantly lead to plastic hinges forming on columns if this ratio exceeds 1.25.
- It is strongly recommended that seismic design regulations should include a new geometrical provision to limit the ratio of beam height to column width, in order to prevent hinge formation on columns.
- The values of effective slab width obtained from the provisions of ACI and EuroCode 8 are not sufficient to ensure the implementation of the weak beam-strong column design methodology.

Acknowledgments

The authors would like to acknowledge the International Institute of Earthquake Engineering and Seismology (IIEES) for supporting this work under grant No. 71412-701.

References

ABAQUS (2013). *Analysis User's Manual 6.10*. Providence, IR: Dassault Systems Simulia Corp. SIMULIA.

ACI (2019). *Building Code Requirements for Structural Concrete, ACI 318-19*. Farmington Hill: American Concrete Institute.

Alfarah, B.F., Almansa, L., & Oller, S. (2017). New methodology for calculating damage variables evolution in plastic damage model for RC structures. *Engineering Structures*, *132*, 70-86.

Arslan, MH., & Korkmaz, HH. (2007). What is to be learned from damage and failure of reinforced concrete 435 structures during recent earthquakes in Turkey? *Engineering Failure Analysis*, *14*(1), 1-22.

Behnam, B. (2018). Parametric finite element analysis of RC wide beam-column connections. *Computers and Structures*, *205*, 28-44.

Dogan, M. (2013). Failure of structural (RC, masonry, bridge) to Van earthquake. *Engineering Failure Analysis*.

Dooley, L., & Bracci, J.M. (2001). Seismic evaluation of column-to-beam strength ratios in reinforced concrete frames. *ACI Structural Journal*, *98*(6), 834-851.

Euro Code 8 (2004). Design of Structures for Earthquake Resistance-Part1: General Rules, Seismic Actions, and Rules for Buildings. Bruxelles.

Haselton, C.B., Liel, A.B., Deierlein, G.G., Dean, B.S., & Chou, J.H. (2011). Seismic collapse safety of reinforced concrete buildings. I: assessment of ductile moment frames. *Journal of Structural Engineering*, *137*(4), 481-491.

Ibarra, L.F., & Krawinkler, H. (2005). *Global Collapse of Frame Structures under Seismic Excitations*. San Francisco: Stanford University, USA, Dissertation.

Iranian National Building Codes, Design and Implantation of RC Buildings, Part 9 (2013).

Kabeyasawa, T., & Kabeyasawa, T. (2018). Effective slab width for evaluating ultimate seismic capacities of reinforced concrete buildings. *Proceedings of the Fourth Congrès International de Géotechnique-Ouvrages-Structures*, Lecture Notes in Civil Engineering 8.

Khalili, A., Kheyroddin, A., Farahani, A., & Sharbatdar, M.K. (2015). Nonlinear behavior of RC frames strengthened with steel curb and prop. *Scientia Iranica International Journal of Science and Technology*, *22*(5), 1712-1722.

Kheyroddin, A., Emami, E., & Khalili, A. (2020). RC beam-column connections retrofitted by steel

prop: experimental and analytical studies. *International Journal of Civil Engineering*, *18*, 501-518.

Kuntz, G.L., & Browning, J. (2003). Reduction of column yielding during earthquakes for reinforced concrete frames. *ACI Structural Journal*, *100*(5), 573-580.

Lee, J., & Fenves, G.L. (1998). Plastic-damage model for cyclic loading of concrete structures. *Journal of Engineering Mechanics*, *124*, 892-900.

Lubliner, J., Oliver, J., Oller, S., & Onate, E. (1989). A plastic-damage model for concrete. *International Journal of Solids Structures*, *25*, 299-326.

Masoudi, M., & Khajevand, S. (2020). Revisiting flexural over strength in RC beam-and-slab floor systems for seismic design and evaluation. *Bulletin of Earthquake Engineering*, *18*, 5309-5541.

Medina, R.A., & Krawinkler, H. (2005). Strength demand issues relevant for the seismic design of moment-resisting frames. *Earthquake Spectra*, *21*(2), 415-439.

Myoungsu, S., & LaFave, J.M. (2004). Seismic performance of reinforced concrete eccentric beam-column connections with floor slabs. *ACI Structural Journal*, *101*(3).

Ning, N., Wenjun, Qu., & Zhongguo J.M. (2014). Role of cast-in situ slabs in RC frames under low frequency cyclic load. *Journal of Engineering Structures*, *59*, 28-38.

Pantazopoulou, S.J., Moehle, J.P., & Shahrooz, B.M. (1988). Simple analytical model for T-beams in flexure. *Journal of Structural Engineering*, *114*(7), 1507-1523.

Pantazopoulou, X. (1991). Response of RC frame under lateral loads. *Journal of Structural Engineering*, *117*(4), 1167-1188.

Paulay, T., & Park, R. (1975). *Reinforced Concrete Structures*. Wiley-Inter science Publication.

Rossetto, T., & Peiris, N. (2009). Observations of damage due to the Kashmir earthquake of October 8, 2005 and study of current seismic provisions for buildings in Pakistan. *Bulletin of Earthquake Engineering*, *7*, 681-899.

Rossetto, T., Peiris, N., & Alarcon, J.E. (2011). Field observations from the Aquila, Italy earthquake of April 6. *Bulletin of Earthquake Engineering*, *9*, 11-37.

Sezen, H., Can Altunisik, A., Emin Arslan, M., Caglar, N., Demir, A., Bektas, N., Dilsiz, A., Gunay, S., Khalil, Z., Marinkovic, M., Safiey, A., Alam, M., Kijewski-Correa, T., & Mosalam, K. (2023). *StEER 2022 Mw 6.1 Duzce, Turkey Earthquake Preliminary Virtual Reconnaissance Report (PVRR). In StEER - November 23 2022, Duzce, Turkey, Mw 6.1 Earthquake*. DesignSafe-CI. https://doi.org/10.17603/ds2-8710-ad45 v1.

Umarani, C., & Ahmed, S. (2014). Analytical investigation on the seismic performance of slabs in RC frame joints. *Magazine of Concrete Research*, *66*(1), 1-19.

Vetr, M., Saeidian, M., & Naserpour, A. (2018). The main reasons for great damages of reinforced concrete buildings on 12th November 2017, Sarpol-e Zahab Earthquake. *Journal of Seismology and Earthquake Engineering*, *20*(3), 73-92.

Yan, B., Huang, L., & Li, D. (2010). Approach of the collapses of RC frame structure school buildings. Earth and Space 2010. *Engineering Science Construction Operation Challenge Environment*, 2653-62.

Zhao, B., Taucer, F., & Rossetto, T. (2009). Field investigation on the performance of building structures during the 12 May 2008 Wenchuan earthquake in China. *Engineering Structures*, *31*(8), 1707-1723.